Sedimentology (2003) **50,** 855–877 doi: 10.1046/j.1365-3091.2003.00586.x

Sequence stratigraphic distribution of diagenetic alterations in coal-bearing, paralic sandstones: evidence from the Rio Bonito Formation (early Permian), southern Brazil

J. MARCELO KETZER*[1], MICHAEL HOLZ†, S. MORAD* and I. S. AL-AASM‡
*Department of Earth Sciences, Uppsala University, Villavägen 16, SE 75236 Uppsala, Sweden (E-mail: marcelo.ketzer@geo.uu.se, jm@ketzer.com.br)
†Instituto de Geociências, UFRGS, Av. Bento Gonçalves 9500, 91501-970 Porto Alegre, Brazil
‡Department of Earth Sciences, University of Windsor, Windsor, Ontario N9B 3P4, Canada

ABSTRACT

Linking siliciclastic diagenesis to sequence stratigraphy allows a better understanding of the parameters controlling the spatial and temporal distribution of diagenetic alterations, and hence of reservoir quality. A study of the coal-bearing, alluvial, deltaic, estuarine and shallow-marine sandstones of the Rio Bonito Formation, early Permian, Paraná Basin (southern Brazil), reveals that the distribution of diagenetic alterations and of related reservoir quality evolution can be constrained within a sequence stratigraphic framework. Calcite, dolomite, siderite, kaolinite and pyrite cementation is consistently linked to sequence and parasequence boundaries, transgressive and maximum flooding surfaces and is systematically distributed within lowstand, transgressive and highstand systems tracts. Diagenesis of coal layers at parasequence boundaries has promoted the formation of stratabound calcite (detectable in resistivity wire line logs), concretionary pyrite and kaolinite and of silicate grain dissolution in sandstones located above and below these boundaries, particularly in the transgressive systems tract. Meteoric water diagenesis caused grain dissolution and the formation of kaolinite in sandstones below sequence boundaries and in lowstand systems tract sandstones. Carbonate bioclasts and low sedimentation rates in lag deposits at parasequence boundaries, transgressive and maximum flooding surfaces favoured the formation of grain-rimming siderite. The results of this study are relevant to the exploration of coal-bed methane and other coal-bearing reservoirs, where it is crucial to unravel and predict the distribution and quality of reservoirs and compartments.

Keywords Coal, diagenesis, sandstone, sequence stratigraphy.

INTRODUCTION

Sequence stratigraphy is a powerful methodology for predicting facies and thus the depositional control on the distribution of reservoirs, seal and source rocks (Posamentier & Allen, 1999). Constraining the distribution of diagenetic alterations (e.g. cementation and dissolution of framework grains) within a sequence stratigraphic framework can considerably improve the ability to predict the spatial distribution and evolution of sandstone reservoirs (Dutton & Willis, 1998; Morad *et al.*, 2000; Ketzer *et al.*, 2003). This approach is well explored in carbonate sequences (Read & Horbury, 1993 and references therein; Tucker, 1993; Moss & Tucker, 1996) but, despite an increasing number of recent studies (Tang *et al.*, 1994; Amorosi, 1995, 1997; Taylor *et al.*, 1995, 2000; Loomis & Crossey, 1996; Dutton & Willis, 1998; South & Talbot, 2000; Ketzer *et al.*,

[1]Present address: IFP (Institut Français du Pétrole) – Divison Géologie-Géochimie, RB40, PB311, 92852 Rueil-Malmaison Cedex, France.

2002), it is still relatively poorly constrained for siliciclastic sequences.

The relationship between sequence stratigraphy and the distribution of diagenetic alterations in sandstones is anticipated because changes in the detrital composition and porewater chemistry often occur at sequence stratigraphic surfaces and within systems tracts (Hart *et al.*, 1992; Morad *et al.*, 2000; Taylor *et al.*, 2000; Taylor & MacQuaker, 2000; Ketzer *et al.*, 2003). Most studies on linking sequence stratigraphy and clastic diagenesis have dealt with the distribution of carbonate cements. Taylor *et al.* (1995), for instance, reported the formation of dolomite concretions in sandstones below parasequence boundaries, transgressive surfaces and maximum flooding surfaces in the Cretaceous rocks of the Book Cliffs, USA. The formation of dolomite was attributed by these authors to the long residence time of the sediments at very shallow depths below the sea floor, owing to the depositional hiatus encountered along these surfaces. Loomis and Crossey (1996) provided a similar explanation for the formation of carbonate concretions at marine flooding surfaces in the Cretaceous sequences in Colorado, USA. Additionally, carbonate cementation along parasequence boundaries in the Carboniferous, Mullaghmore Formation of NW Ireland (Ketzer *et al.*, 2002) and on top of regressive units in the Eocene fan-delta complex of Sant Llorenç del Munt, Ebro Basin, Spain (South & Talbot, 2000), was attributed to the presence of carbonate bioclastic lags, which acted as both source and nuclei for cementation. Carbonate cementation is also favoured along parasequence boundaries because of the low sedimentation rates and, thus, prolonged residence time of the sediment on the sea floor, therefore enhancing the diffusive flux of calcium and carbonate ions from the overlying sea water (Kantorowicz *et al.*, 1987; Taylor *et al.*, 1995; Loomis & Crossey, 1996; Klein *et al.*, 1999). Changes in porewater chemistry and, hence, in the chemical and isotopic composition of carbonate cements owing to changes in relative sea level have been reported in the Cardium Formation (Hart *et al.*, 1992), in the Triassic Buntsandstein, Spain (Morad *et al.*, 1992), and in the Upper Cretaceous Marshybank Formation, Canada (McKay *et al.*, 1995).

Attempts have also been made by some authors to link the distribution of clay minerals to the sequence stratigraphic framework of clastic deposits (Ketzer *et al.*, 2003). The formation of clay minerals appears to be linked mainly to parasequence boundaries, and particularly to maximum flooding surfaces. Amorosi and Centineo (2000) reported that the concentration of glaucony in the Tertiary sequences of the Boulognais region, NW France, increases upwards within the transgressive systems tracts towards the maximum flooding surfaces. This increase in glaucony was attributed by these authors to the long residence time and reduced sediment supply encountered during transgression. Permeable sandstones below subaerially exposed sequence boundaries are subjected to mechanical clay infiltration in a semi-arid climate, or pervasive kaolinitization resulting from percolation of undersaturated meteoric water in a humid climate (Ketzer *et al.*, 2003).

The aim of this paper is to elucidate and discuss the distribution of diagenetic alterations in coal-bearing, paralic (deltaic, coastal and shallow-marine) sandstones of the Rio Bonito Formation, early Permian, in the context of sequence stratigraphy. The influence of peat/coal layers on the diagenesis of siliciclastic deposits is well documented in the literature (Matsumoto & Iijima, 1981; Curtis & Coleman, 1986). As the distribution of peat/coal layers is linked to changes in relative sea level, unravelling their influence on the distribution of diagenetic alterations in siliciclastic deposits can be better refined if made within a sequence stratigraphic context. The availability of a large number of drill cores and outcrops, and of a high-resolution sequence stratigraphic framework of the Rio Bonito Formation (Holz, 1999; Holz *et al.*, 2002) makes this study feasible. Such detailed study will ultimately help to develop more comprehensive and precise conceptual, predictive models for the distribution of clastic reservoirs and diagenetic seals. The Rio Bonito Formation is a potential analogue for the study of other coal-bearing, reservoir successions in which detailed distribution of reservoir and seals is of great importance, such as in coal-bed methane projects.

Diagenetic regimes used in the paper are: (1) eodiagenesis (< 70 °C), during which porewater chemistry is controlled by surface waters (i.e. depositional and/or meteoric waters); and (2) mesodiagenesis (> 70 °C), mediated by evolved formation waters (Morad *et al.*, 2000).

STUDY AREA AND GEOLOGICAL SETTING

The study area is located at the south-eastern margin of the Paraná Basin, which is a large

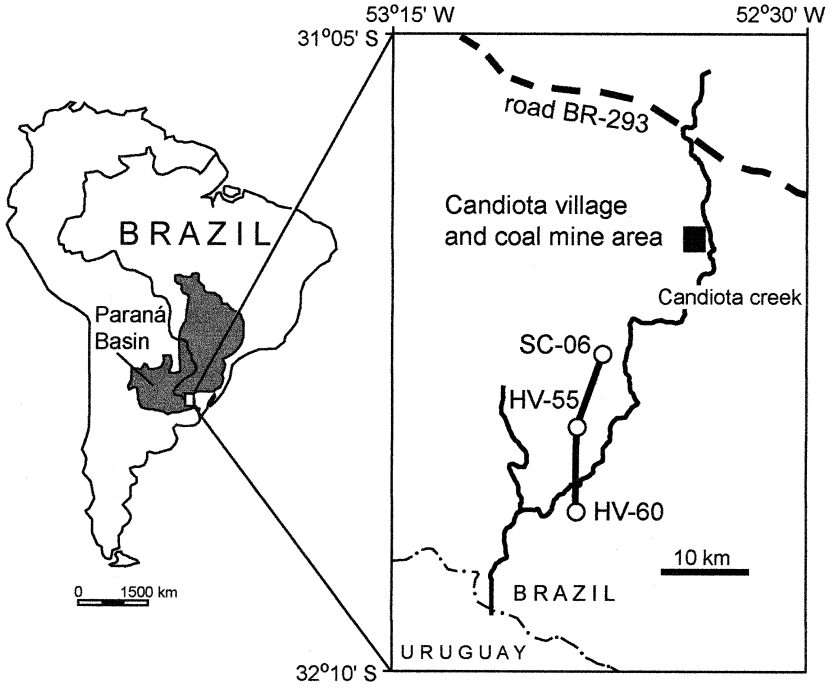

Fig. 1. Location map of the Paraná Basin showing the studied area in southern Brazil. Samples used for this study are from wells SC-06, HV-55 and HV-60, and from outcrops along the road BR-293.

(1 400 000 km^2) intracratonic basin covering part of southern Brazil, Paraguay, Uruguay and Argentina (Fig. 1). Subsidence of the basin combined with Palaeozoic sea-level changes created five second-order sequences (Zalan *et al.*, 1990). The studied stratigraphic interval comprises part of the Rio Bonito Formation, which belongs to the Permo-Carboniferous sequence.

The Rio Bonito Formation consists of interbedded sandstones, mudstones and coals, deposited in paralic environments (deltaic, estuarine and shallow marine) during the early Permian (Artinskian to Kungurian, 268–258 Ma; Daemon & Marques-Toigo, 1991). Deposition occurred under cold and humid conditions (Patzkowsky *et al.*, 1991), at a palaeolatitude of ≈41°S (Smith *et al.*, 1981). The coal deposits are composed of arborescent and herbaceous plant material, which accumulated in coastal swamps (Alves & Ade, 1996; Holz *et al.*, 2002). Coal deposits of the Rio Bonito Formation in the study area comprise Brazil's largest coal reserve.

The Rio Bonito Formation is commonly intruded by basaltic dikes and sills, which are coeval to the volcanic Serra Geral Formation (late Jurassic to early Cretaceous, 147–119 Ma; Zalan *et al.*, 1990). Vitrinite reflectance measured in coal layers of the study area revealed R_0 values between 0·42 and 0·56 (Holz *et al.*, 2002), which correspond to maximum temperatures of about 100 °C (Bustin *et al.*, 1977). Present-day maximum burial depth of the studied interval is 350 m.

DEPOSITIONAL FACIES AND SEQUENCE STRATIGRAPHY

In the Paraná Basin, the early Permian was a period of overall transgression related to a second-order relative sea-level rise (cf. Vail *et al.*, 1977) and a transgression of the shoreline punctuated by short regressive episodes (Zalan *et al.*, 1990). Deposition began in a restricted, funnel-shaped, tidally influenced estuarine bay, bordered by basement highs, and ended in epeiric seashore (Holz *et al.*, 2002; Fig. 2). The studied interval comprises part of two third-order sequences described by Holz (1999) and Holz *et al.* (2002), which are hereafter referred to as lower and upper sequences (Fig. 3). The main depositional facies in these two sequences are described in Table 1. The lower sequence (≈ 80 m thick) is composed of: (1) a lowstand systems tract (LST) with deltaic and rare alluvial fan deposits; (2) a transgressive systems tract (TST) with estuarine and shallow-marine (foreshore, upper and lower shoreface) deposits; and (3) a highstand systems tract (HST) with upper and lower shoreface deposits (Fig. 3). The basal sequence boundary is a flat, erosive surface without valley incision (Holz *et al.*, 2002). Likewise, the transgressive

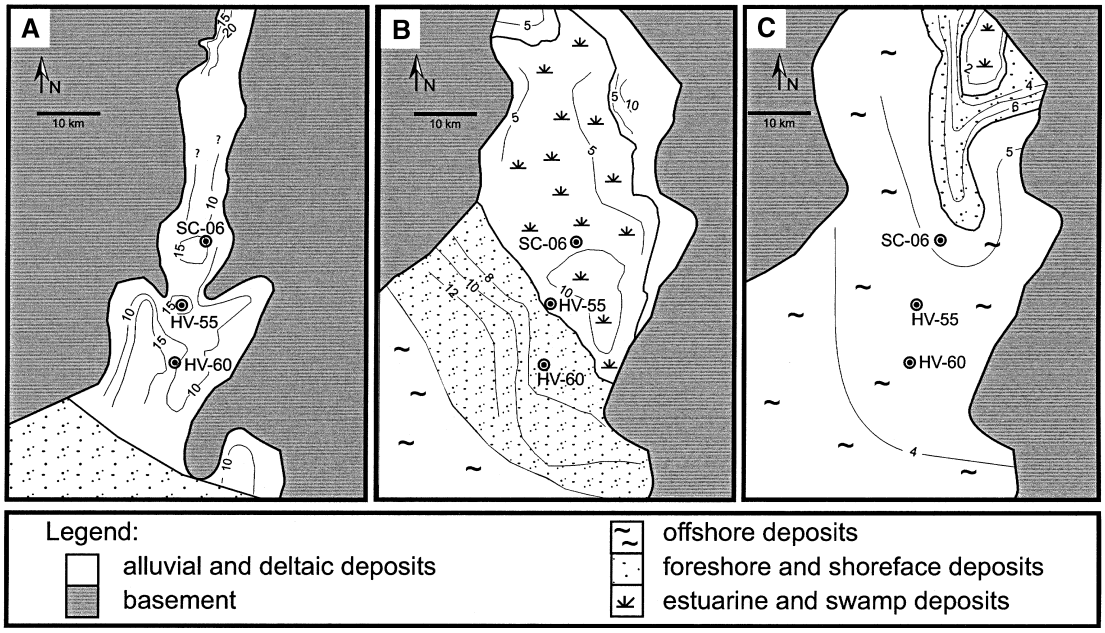

Fig. 2. Palaeogeographic reconstruction of depositional environments of the Rio Bonito Formation during the early Permian in the Paraná Basin. Deposition started in a narrow estuary and ended in an epeiric seashore. (A) and (B) correspond to the lowstand and transgressive systems tract of the lower sequence, respectively, and (C) corresponds to the lowstand systems tract of the upper sequence (see Fig. 3). Reconstruction is based on correlation of 60 wells. Studied wells (SC-06, HV-55 and HV-60) are plotted.

surface (TS) is flat and erosive, and locally marked by *Glossifungites* burrows (Holz *et al.*, 2002). Parasequence boundaries of the TST are commonly marked by estuarine or shoreface sandstones that overlie coal deposits (Fig. 4A). The retrogradational stacking pattern of the TST parasequence set is clearly identified by the backstepping pattern of the coal layers (Fig. 3). The TST contains the most important coal deposits of the Rio Bonito Formation. Some minor coal deposits also occur in the upper LST. Conglomeratic transgressive lag deposits are rare and occur at parasequence boundaries and at the transgressive surface. Most of the HST of the lower sequence is absent as a result of non-deposition and/or erosion during formation of the upper sequence boundary (Holz *et al.*, 2002; Fig. 3). This boundary, which marks the base of the upper sequence ($\approx$ 40 m thick), is a flat surface showing no evidence of valley incision, and is marked by a conglomeratic lag deposit (Holz *et al.*, 2002; Fig. 3). Only the LST and the lower part of the TST of the upper sequence are present within the studied interval (Fig. 3). The LST comprises lower shoreface deposits, whereas the TST comprises lower shoreface and offshore deposits (Table 1). The transgressive surface and parasequence boundaries in both LST and TST are marked by conglomeratic or bioclastic lag deposits (Fig. 4B). The transgressive surfaces can be marked in outcrop by the presence of weathering-resistant layers (Fig. 4C).

SAMPLES AND METHODS

A total of 115 representative core samples were collected from three wells (SC-06, HV-55 and HV-60). These wells were selected in order to represent proximal, intermediate and distal deposits, respectively, in a stratigraphic section perpendicular to the palaeoshoreline (Fig. 3). Twelve sandstone samples were also collected in three outcrops along the road BR-293 and in the Candiota Coal Mine (Fig. 1), which are in a more proximal location relative to the studied wells. Sampling focused on sequence stratigraphic surfaces (sequence and parasequence boundaries, transgressive surface and maximum flooding surface) and on representative sandstones from the systems tracts. A total of 110 sandstone samples were selected for preparation of colour epoxy-impregnated thin sections. Modal composition of sandstones was obtained from 56 samples by counting 300 points in each thin section. Outcrop samples were not included because of the considerable influence of weathering.

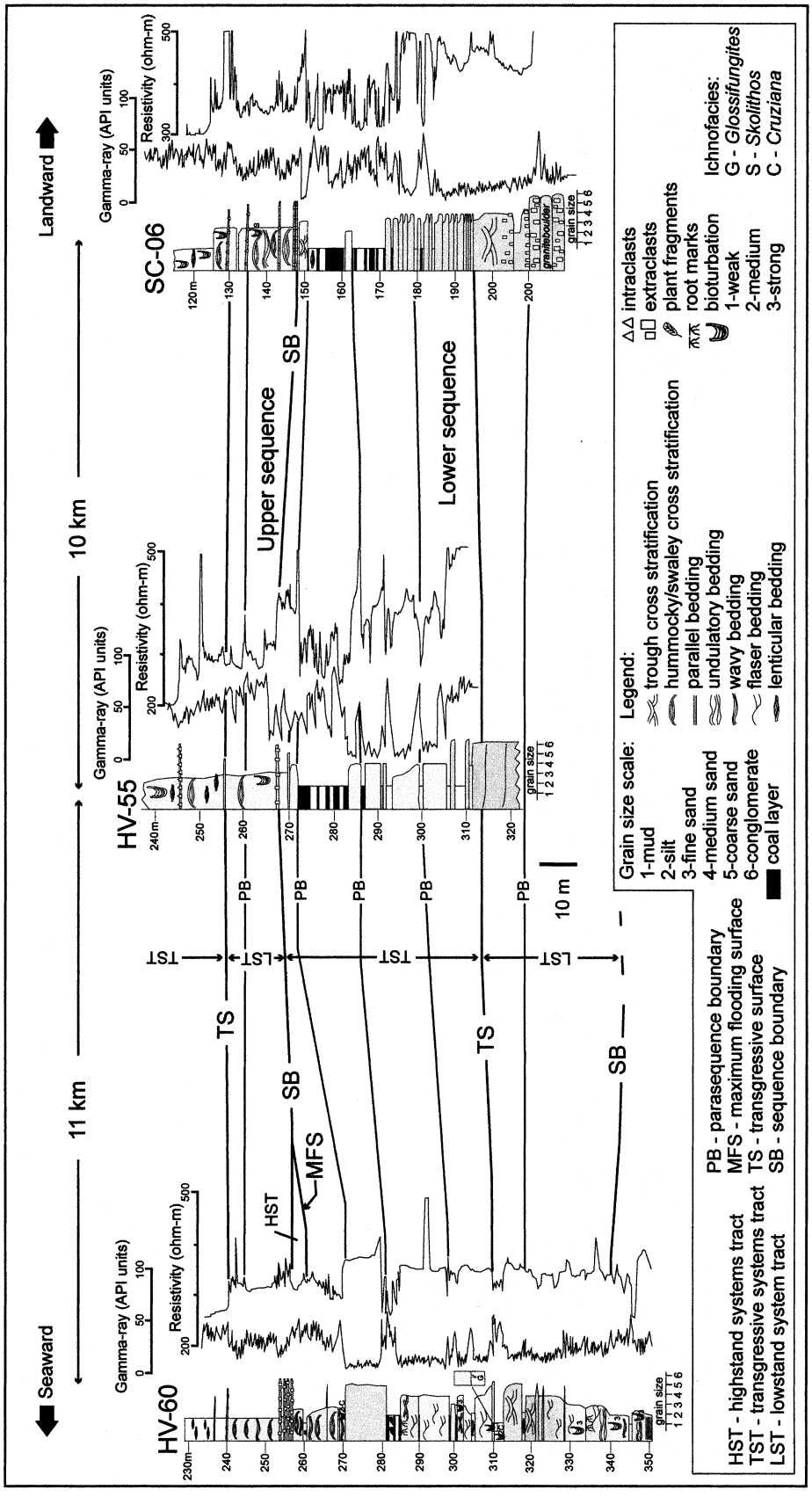

Fig. 3. Stratigraphic section of the studied interval of the Rio Bonito Formation showing well correlation, sequence and parasequence boundaries and systems tracts. The section is approximately perpendicular to the palaeoshoreline (see Figs 1 and 2 for location).

Table 1. Depositional systems and lithofacies description of the Rio Bonito Formation.

Depositional system	Subsystem	Lithofacies description	Occurrence
Alluvial		Matrix- and clast-supported conglomerates	Proximal LST of the lower sequence
Deltaic	Distributary channel	Medium- to coarse-grained sandstones with trough cross-bedding	LST of the lower sequence
	Interdistributary bay	Muddy sandstones with coals	
	Proximal distributary mouth bar		Medium-grained sandstones, massive or with trough cross-bedding
	Distal distributary mouth bar	Fine- to medium-grained sandstones with trough cross-bedding	
	Very distal mouth bar and prodelta	Mudstones and siltstone with parallel bedding	
Estuarine	Proximal bayhead delta	Coarse-grained sandstones with trough cross-bedding, rare conglomerates	TST of the lower sequence
	Distal bayhead delta	Fine-grained sandstone with trough cross-bedding, mudstone with lenticular bedding	
	Tidal sand bars/tidal delta	Sandstones with drape and flaser bedding, some trough cross-bedding	
	Muddy and sandy tidal flats	Laminated mudstones and siltstones, common sandstones with drape and flaser bedding and trough cross-bedding	
	Marshes and swamps	Coal seams and coaly mudstones	
	Washover fans	Conglomerates (including intraclastic) and trough cross-bedded sandstones	
Shallow marine	Foreshore	Medium-grained sandstones with swash cross-stratification	TST and HST of the lower sequence, LST and TST of the upper sequence
	Upper shoreface	Coarse-grained sandstone with trough cross-bedding	
	Middle shoreface	Medium- to fine-grained sandstones with hummocky cross-bedding, some wavy bedding	
	Lower shoreface to offshore	Laminated mudstones and some fine-grained sandstones with hummocky cross-bedding	

LST, TST and HST refer to lowstand, transgressive and highstand systems tracts, respectively.

Chemical analyses of carbonates and silicates were performed in a Cameca Camebax BX50 electron microprobe (EMP), equipped with a backscattered electron detector (BSE). Operation conditions included an acceleration voltage of 20 kV, a beam current of 8 nA for carbonates and 12 nA for silicates and a beam spot size of 1–5 μm. The standards and counting times used were: wollastonite (Ca, 10 s), orthoclase (K, 5 s), albite (Na, Si, 5 and 10 s respectively), corundum (Al, 20 s), MgO (Mg, 10 s), $MnTiO_3$ (Mn, 10 s) and haematite (Fe, 10 s). Precision of analysis was better than 0·1 mol%. Analytical totals of carbonates (93–102%) were normalized to 100%. Ten representative thin sections of calcite-cemented sandstones were analysed using a Technosyn 8200 Mk II cold cathodoluminoscope. Operation conditions included 15–20 kV acceleration voltages and 0·35–0·45 mA beam currents.

A Jeol JSM-T330 scanning electron microscope (SEM) was used to investigate habits and paragenetic relationships among diagenetic minerals in 32 sandstone samples. Operation conditions

Fig. 4. (A) Parasequence boundary (arrow) of the transgressive systems tract of the lower sequence, marked by shoreface sandstones (light grey) on top of coal and coaly mudstones deposited in coastal swamps (dark grey). (B) Bioclastic lag deposit associated with TST parasequence boundaries of the upper sequence. (C) Outcrop showing the transgressive surface (TS) separating lowstand systems tract from transgressive systems tract in the upper sequence. The transgressive surface is marked by a weathering-resistant horizon (arrow).

included 20 kV acceleration voltage and 0·4 nA beam current.

Stable isotope analyses of carbon and oxygen were performed on 18 carbonate-cemented sandstone samples. Microsampling using microdrilling techniques was attempted to obtain carbonate cements with different textures. However, the small size of the pores and particles led to contamination among the different generations of carbonate cements. Therefore, all analyses represent bulk-rock measurements. Samples containing calcite, ankerite and siderite were subjected to the sequential chemical separation treatment described by Al-Aasm *et al.* (1990). Calcite-cemented samples were reacted with 100% phosphoric acid at 25 °C for 4 h, and ankerite- and siderite-cemented samples were reacted at 50 °C for 24 h and 96 h respectively. The CO_2 gas was analysed using a SIRA-12 mass spectrometer. The phosphoric acid fractionation factors used were 1·01025 for calcite, 1·01060 for ankerite and 1·010454 for siderite. Precision of all analyses was better than ±0·05‰. Oxygen and carbon isotope data are presented in the δ notation relative to the Vienna PDB (Peedee Belemnite) and SMOW (standard mean ocean water) standards.

DETRITAL COMPOSITION OF SANDSTONES

Modal composition of the sandstones from various systems tracts is summarized in Table S1 (see *Supplementary material*). The LST deltaic and the TST estuarine sandstones are subarkoses, whereas the TST and HST foreshore and shoreface sandstones are subarkose to quartzarenites (Fig. 5). Conglomeratic lag deposits at parasequence boundaries and at transgressive surfaces and sequence boundaries are sublitharenites in composition (Fig. 5). Quartz grains are dominantly monocrystalline, and K-feldspar dominates over plagioclase in all facies and systems tracts (Table S1). Lithic fragments are igneous (mainly acid plutonic, but also basic and acid volcanic types), metamorphic (quartzite, schist and gneiss) and rarely sedimentary (fine-grained sandstones) in origin (Table S1). Micas (biotite and muscovite), heavy minerals (tourmaline, epidote, zircon and garnet), opaque minerals and glaucony are only minor constituents in all sandstones types (Table S1). Rarely, however, glaucony content reaches up to 5 vol% in TST shoreface sandstones (Table S1). Glaucony is slightly evolved ($K_2O = 4{\cdot}5$ wt%; cf. Odin & Matter, 1981) and occurs as scattered, commonly rounded pellets (up to 250 μm across). In thin section, these pellets may display cracks (Fig. 6A) and resemble the parautochthonous glaucony assemblage described by Amorosi (1995, 1997). Other detrital constituents in the sandstones are: (1) sand-sized coal fragments, which occur in the sequence boundary and TST parasequence boundary lag deposits of the upper sequence; and (2) carbonate bioclasts, which occur only in the shoreface sandstones (traces) and in the parasequence boundary lag deposits. Pseudomatrix, which is formed by the deformation of ductile mud clasts, is an important constituent in the TST estuarine sandstones and occurs as a minor constituent in transgressive surface lag deposits (Table S1).

PETROGRAPHY, GEOCHEMISTRY AND DISTRIBUTION OF DIAGENETIC MINERALS

Pyrite

Pyrite occurs mainly as concretions of irregular shape (2–10 cm in diameter; Fig. 6B), composed of framboidal, microcrystalline ($\approx 0{\cdot}5$ μm) and blocky (10–200 μm) cubic crystals. Microcrystalline pyrite displays collomorphic texture composed of framboidal pyrite aggregates in the centre and an alternation of microcrystalline pyrite and anhydrite aggregates at the margin (Fig. 6C). Blocky pyrite engulfs, and thus postdates, microcrystalline pyrite aggregates (Fig. 6D) and partially or completely replaces framework grains, calcite, pseudomatrix, and quartz overgrowths (Fig. 6E). Blocky pyrite also fills large pores in sandstones without quartz overgrowths (Fig. 6F). Pyrite concretions occur in TST estuarine and foreshore sandstones of the lower sequence that under- or overlie coal layers below parasequence boundaries (Fig. 7). Pyrite replaces coal fragments that occur as lag deposits along sequence and TST parasequence boundaries.

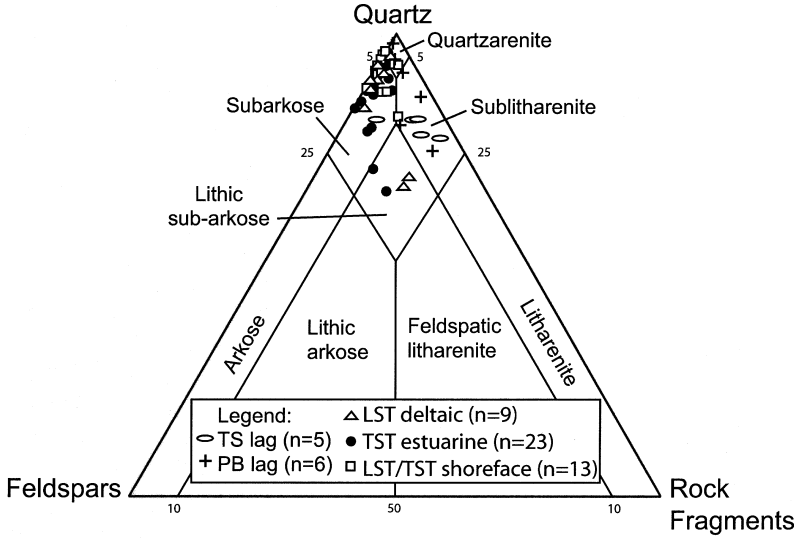

Fig. 5. Detrital composition of 56 sandstone samples plotted on McBride's (1963) classification diagram. LST, TST and HST refer to lowstand, transgressive and highstand systems tracts respectively. TS and PB refer to transgressive surface, sequence boundary and parasequence boundary respectively.

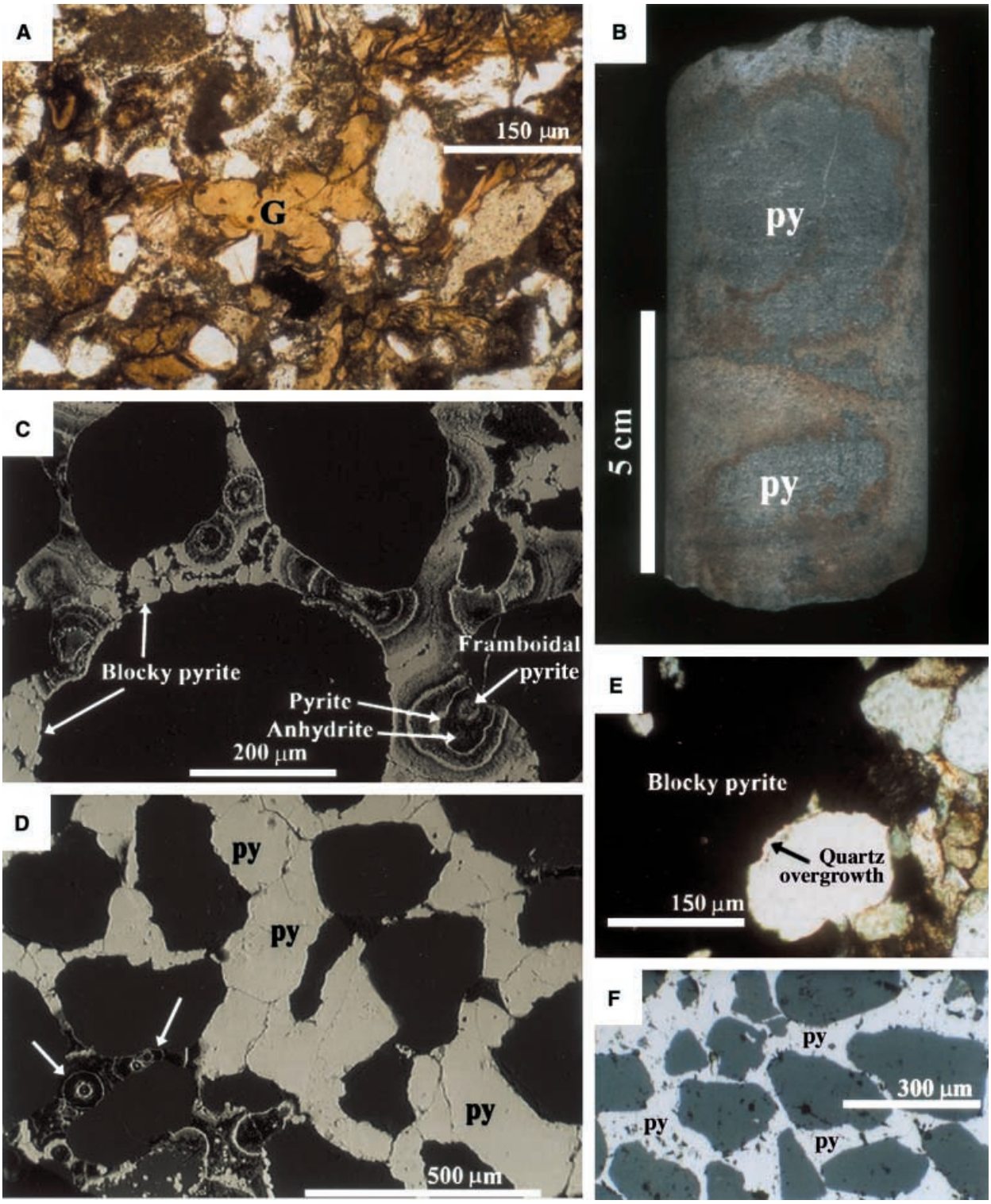

Fig. 6. (A) Photomicrograph (crossed nicols) showing a glaucony pellet (G) with preserved cracks. (B) Core sample (SC-06, 150·9 m) with pyrite concretions. (C) BSE image showing the colloform-like texture of microcrystalline pyrite and anhydrite. (D) BSE image showing blocky pyrite crystals (py), which nucleated on microcrystalline pyrite aggregates (arrows). (E) Photomicrograph (crossed nicols) showing blocky pyrite partially replacing quartz overgrowth. (F) Photomicrograph (reflected light) showing blocky pyrite crystals filling large pores in sandstones.

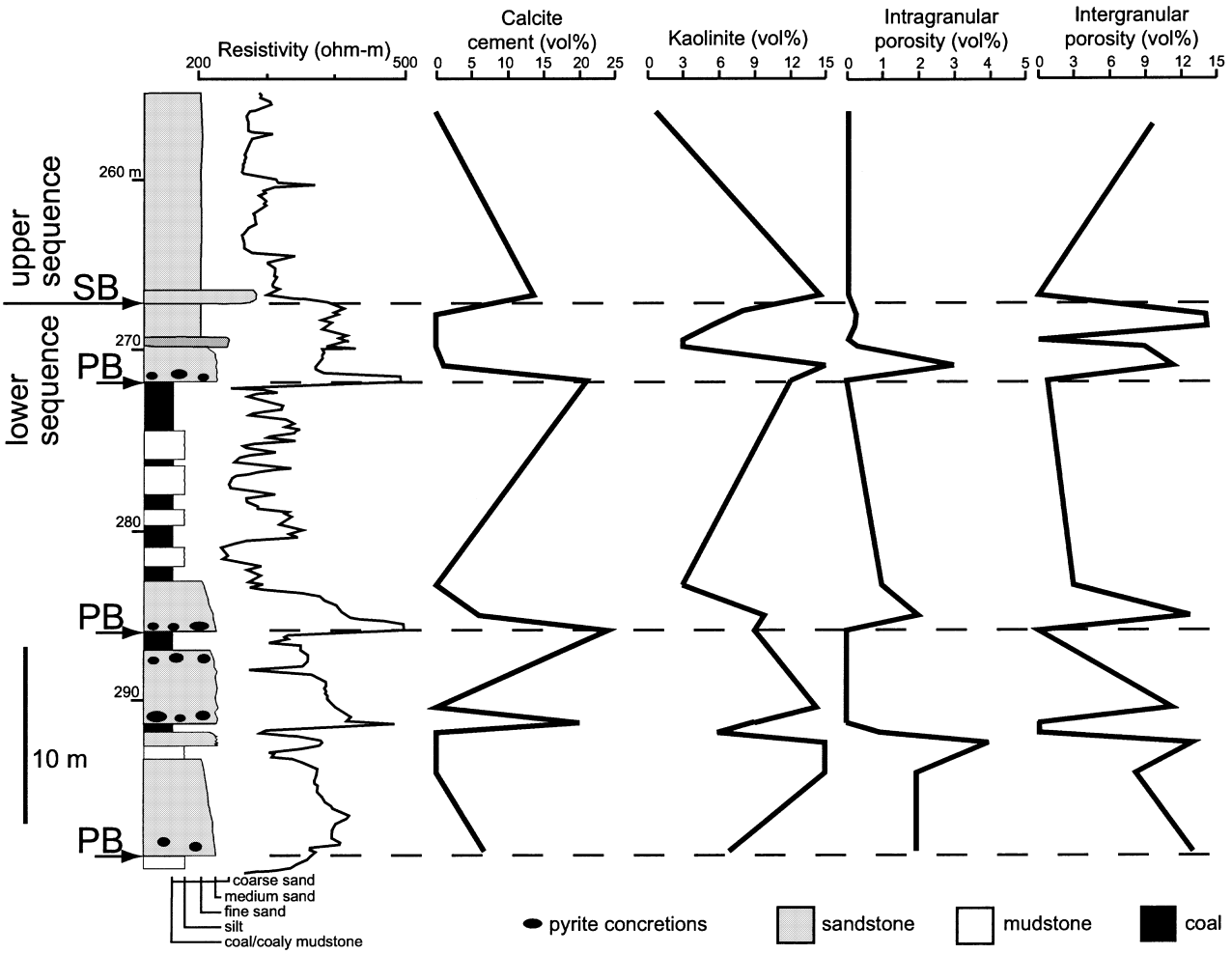

Fig. 7. Diagram showing the distribution of calcite, kaolinite, intragranular porosity and intergranular porosity in TST estuarine and shoreface sandstones of the lower sequence, and LST shoreface sandstones of the upper sequence (well HV-55). Note that peaks of high resistivity in the wireline logs correspond to tightly cemented calcite (≥ 20 vol%) sandstones above parasequence boundaries and coal layers of the lower sequence. Pyrite concretions occur in sandstones above and below coal layers in the vicinity of parasequence boundaries.

Calcite

Calcite (microcrystalline, poikilotopic and mosaic) occurs as pore-filling cement, which partially or totally replaces detrital quartz, feldspar and rock fragments. Microcrystalline calcite occurs in trace amounts and forms aggregates around detrital grains (Fig. 8A) in shoreface sandstones above parasequence boundaries of the TST. Poikilotopic calcite fills either large intergranular pores of loosely packed sandstones (intergranular volume > 25%) lacking quartz overgrowths (Fig. 8B) or small pores in tightly packed sandstones (intergranular volume < 25%), engulfing, and hence post-dating, quartz overgrowths (Fig. 8C). The former calcite engulfs, and thus post-dates, microcrystalline calcite and kaolinite, whereas the latter calcite engulfs, and thus post-dates, kaolinite, siderite and ankerite (Fig. 8D). Both calcites engulf, but are also engulfed and replaced by, blocky pyrite, suggesting a contemporaneous formation. Cathodoluminescence examinations revealed blotchy, bright orange to dull red luminescence in all calcites. Poikilotopic calcite occurs in almost all facies and systems tracts (Table S1), but is particularly linked to parasequence boundaries containing coal layers, which occur in the estuarine, foreshore and shoreface sandstones. Such calcite forms stratabound cement that is closely associated with pyrite concretions (Fig. 7). The extent of calcite cementation at parasequence boundaries varies from pervasive (> 20 vol%) within the first metre above parasequence boundaries to patchy

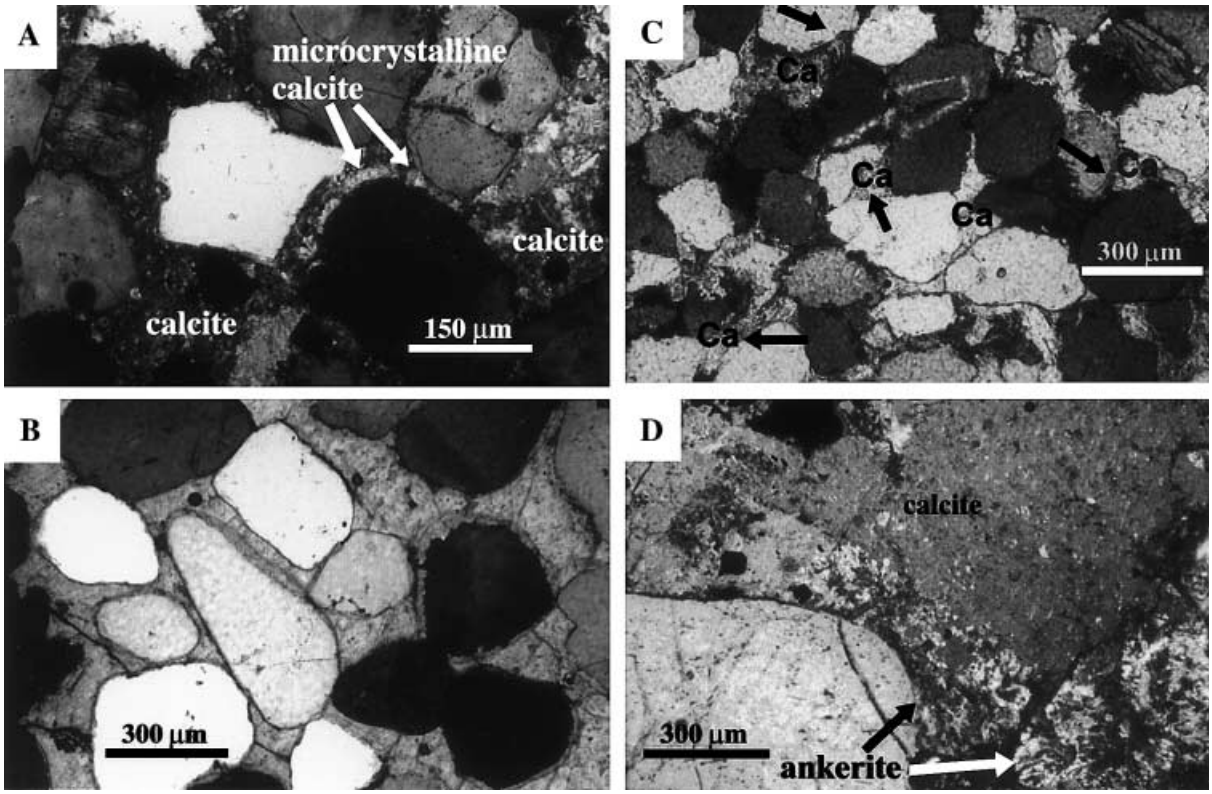

Fig. 8. (A) Photomicrograph (crossed nicols) showing microcrystalline calcite as aggregates around detrital grains, which are engulfed by pore-filling calcite. (B) Photomicrograph (crossed nicols) showing poikilotopic calcite filling large pores in sandstones lacking quartz overgrowth. (C) Photomicrograph (crossed nicols) showing poikilotopic calcite (Ca) filling small pores in sandstones after quartz overgrowth (arrows). (D) Photomicrograph (crossed nicols) showing poikilotopic calcite covering ankerite.

(< 5 vol%) further up in the same parasequence (Fig. 7). Such extensive calcite cementation near the parasequence boundary is recognized in resistivity logs because of the high resistivity values (e.g. ≈ 500 ohm-m) encountered. Progressively lower resistivity values (down to ≈ 350 ohm-m) are encountered upwards, owing to the decrease in the amounts of calcite cement (Fig. 7).

All types of calcite are nearly pure $CaCO_3$ (Table 2), with only minor quantities (≈ 1 mol%) of $MnCO_3$ and $FeCO_3$. The contents of $MgCO_3$ and $SrCO_3$ are below the detection limit. Bulk-rock, carbon and oxygen isotopes reveal a range of $\delta^{13}C_{VPDB}$ between −7·7‰ and −3·6‰, and $\delta^{18}O_{VPDB}$ between −16·7‰ and −8·2‰ (Table 2).

Ankerite

Ankerite occurs as coarse (up to 200 μm), blocky crystals displaying wavy extinction, filling intergranular pores or replacing organic fragments, pseudomatrix or detrital grains. Ankerite engulfs and covers, and thus post-dates, kaolinite and quartz, but is engulfed by, and thus predates, poikilotopic calcite. Ankerite occurs in small amounts in LST, TST and HST estuarine, foreshore and shoreface sandstones but is absent in LST deltaic sandstones (Table S1). Ankerite is also common in the transgressive surface, parasequence and sequence boundary lag deposits (Table S1), where it replaces coal fragments. Ankerite (average $Fe_{0·21}Mg_{0·21}Mn_{0·02}Ca_{0·56}CO_3$; Table 2) displays a patchy zonation in BSE images, which results from variations in the $FeCO_3$ content (8–28 mol%). The $\delta^{13}C_{VPDB}$ values vary between −4·7‰ and −3·3‰, and $\delta^{18}O_{VPDB}$ values vary between −7·5‰ and −12·5‰ (Table 2).

Siderite

Siderite occurs as small (10–15 μm), prismatic or rhombic crystals (Fig. 9A) that form fringes around carbonate bioclast grains (Fig. 9B) or fill intragranular pores in the LST shoreface sandstones, parasequence boundary and transgressive surface lag deposits of the upper sequence (Table S1). Siderite is engulfed by, and thus

Table 2. Elemental and stable carbon and oxygen isotope composition of calcite, ankerite and siderite.

Well/sample	$MgCO_3$	$CaCO_3$	$MnCO_3$	$FeCO_3$	$\delta^{13}C_{VPDB}$	$\delta^{18}O_{VPDB}$	Occurrence
Calcite							
Well SC-06							
150·9 m	bdl	98·34	0·4	1·15	−5·76	−10·45	Shoreface sandstone (PB)
	bdl	97·99	0·71	1·08			
	bdl	98·12	0·53	1·21			
	bdl	98·27	0·18	1·55			
	bdl	98·97	0·51	0·52			
150 m	bdl	99·66	0·05	0·22	−7·73	−8·22	Shoreface sandstone (PB)
	bdl	98·51	0·56	0·92			
	bdl	98·21	0·51	1·06			
	bdl	98·53	0·52	1·07			
144·8 m	bdl	97·56	0·66	1·78	−5·29	−11·09	Parasequence boundary lag
136·9 m	bdl	99·09	0·42	0·49	−6·03	−10·95	Shoreface sandstone
	bdl	98·67	0·04	1·29			
129·8 m	bdl	97·11	1·33	1·56	−7·58	−10·45	Parasequence boundary lag
Well HV-60							
331·3 m					−5·43	−10·89	Deltaic sandstone
329·5 m	bdl	96·59	3·28	0·13	−5·00	−10·59	Deltaic sandstone
	bdl	97·43	2·57	bdl			
	bdl	97·49	2·93	0·06			
297 m					−5·58	−15·10	Estuarine sandstone
296 m					−7·09	−9·01	Estuarine sandstone
279·05 m	bdl	99·09	0·81	0·09	−6·1	−10·07	Shoreface sandstone (PB)
	bdl	98·21	1·66	0·08			
	bdl	97·85	1·68	0·47			
265·5 m	bdl	97·13	0·57	2·29	−3·58	−11·19	Shoreface sandstone
	bdl	96·68	0·54	2·78			
254·2 m	bdl	95·21	3·91	0·88	−6·20	−8·72	Sequence boundary lag
	bdl	96·03	3·21	0·77			
Well HV-55							
309·8 m	bdl	98·11	0·78	1·11	−4·18	−8·64	Deltaic sandstone
	bdl	97·04	2·34	0·62			
	bdl	97·51	0·93	1·44			
	bdl	97·46	2·17	0·37			
	bdl	97·31	1·97	0·64			
288·8 m					−5·07	−11·45	Shoreface sandstone
287·65 m	bdl	99·17	0·29	0·45			Shoreface sandstone (PB)
273·2 m	bdl	98·65	1·13	0·22	−4·83	−11·42	Shoreface sandstone (PB)
261 m					−5·58	−16·69	Sequence boundary lag
Ankerite							
Well SC-06							
143·4 m	25·82	52·19	1·78	20·21	−3·51	−10·71	Parasequence boundary lag
	15·84	53·47	3·22	27·47			
	13·79	56·82	2·6	26·78			
	25·49	55·42	0·32	18·73			
	14·19	53·98	3·68	28·15			
	20·49	54·99	2·12	22·18			
	23·42	54·33	1·71	20·54			
	14·97	53·85	3·11	28·07			
136·9 m	22·12	60·11	0·34	17·05			Shoreface sandstone
	19·37	53·63	2·92	24·08			
134·05 m	25·01	59·01	0·22	15·31			Parasequence boundary lag
	14·83	54·09	3·70	26·49			
Well HV-60							
265·5 m					−3·28	−12·46	Shoreface sandstone
254·2 m	23·78	60·54	0·22	15·33			Sequence boundary lag
	17·79	59·62	1·33	21·26			
	22·41	57·85	0·63	19·11			

Table 2. Continued.

Well/sample	$MgCO_3$	$CaCO_3$	$MnCO_3$	$FeCO_3$	$\delta^{13}C_{VPDB}$	$\delta^{18}O_{VPDB}$	Occurrence
Well HV-55							
287·65 m	33·86	56·99	1·21	7·95	−4·49	−7·49	Shoreface sandstone (PB)
	24·84	56·49	1·55	16·87			
	28·81	55·55	1·25	13·7			
273·2 m	17·54	55·48	2·55	24·39	−4·76	−7·41	Shoreface sandstone (PB)
271·4 m					−4·67	−9·98	Shoreface sandstone
269·1 m	19·15	53·16	0·17	27·53	−4·48	−8·57	Shoreface sandstone
	24·34	52·31	2·87	20·49			
Siderite							
Well SC-06							
144·8 m	15·79	3·46	2·96	77·78	−5·11	−12·18	Parasequence boundary lag
	0·62	2·43	3·28	93·66			
143·4 m	0·22	3·32	14·78	81·69			Parasequence boundary lag
	9·39	2·59	3·76	84·27			
129·8 m	0·49	4·51	2·41	92·58			
	0·62	4·19	1·42	93·76			
	0·27	4·75	2·74	92·24			
	14·51	3·45	1·21	80·77			
	19·07	3·31	0·19	77·47			
	0·21	4·25	3·17	92·37			
	25·1	1·36	0·15	73·39			
	7·88	1·48	7·82	83·40			

PB refers to sandstones in the vicinity of a parasequence boundary. Elemental analyses are mol% and stable isotopes are per mil. bdl, below detection limit.

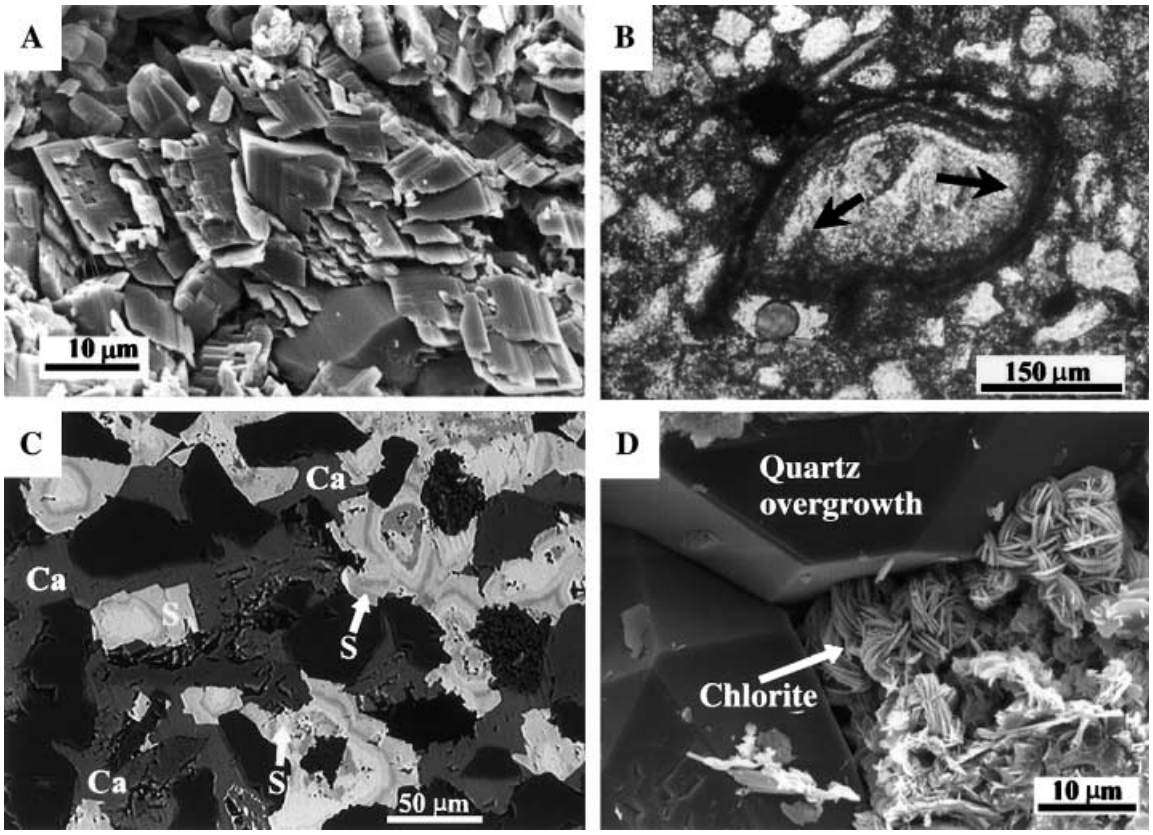

Fig. 9. (A) SEM image showing rhombic siderite crystals with curved faces. (B) Photomicrograph (crossed nicols) showing siderite crystals (arrows) as fringes around a bioclast grain. (C) BSE image showing zoned siderite crystals (S) engulfed by calcite (Ca). (D) SEM image showing chlorite aggregates engulfed by quartz overgrowths.

post-dates, poikilotopic calcite. Siderite crystals are compositionally zoned (Fig. 9C) owing to variations in $MgCO_3$ contents, which range from 24·8 mol% in the core to nearly zero at the rims (average $Fe_{0·85}Mg_{0·08}Mn_{0·04}Ca_{0·03}CO_3$; Table 2). Owing to its small amounts, isotopic analyses of siderite were not possible to perform, except for one sample (Table 2).

Chlorite

Chlorite is a minor and rare constituent of the studied sandstones (Table S1). It occurs as grain-coating platelets arranged perpendicularly to grain surfaces, as pore-filling aggregates showing a rosette-like texture or as scattered platelets within pseudomatrix and micas. EMP analyses of chlorite reveal a composition that is close to the chamosite ($Mg_{1·1}Fe_{7·6}Al_{2·9}(Si_{5·8}Al_{2·2})O_{20}(OH)_{16}$). Chlorite is engulfed by, and thus predates, quartz overgrowths and calcite (Fig. 9D). Chlorite was detected in two samples (TST shoreface sandstone and sequence boundary lag deposit), and thus its distribution pattern cannot be linked precisely to facies or sequence stratigraphy.

Kaolinite

Kaolinite occurs as booklets and vermicular aggregates (Fig. 10A) that fill intergranular pores or replace micas, glaucony, pseudomatrix and feldspars. Kaolinitized micas display expanded textures (Fig. 10B). Extensively kaolinitized feldspars are collapsed and squeezed into open pores (Fig. 10C). Kaolinite is engulfed by, and thus post-dates, quartz overgrowths, poikilotopic calcite (Fig. 10D) and ankerite. Kaolinite is abundant in the LST deltaic deposits, and is also a common constituent in the TST estuarine and LST and TST foreshore and shoreface sandstones (Table S1). An increase in kaolinite content in shoreface sandstones occurs below TST parasequence boundaries containing coal layers and below sequence boundaries (Fig. 7).

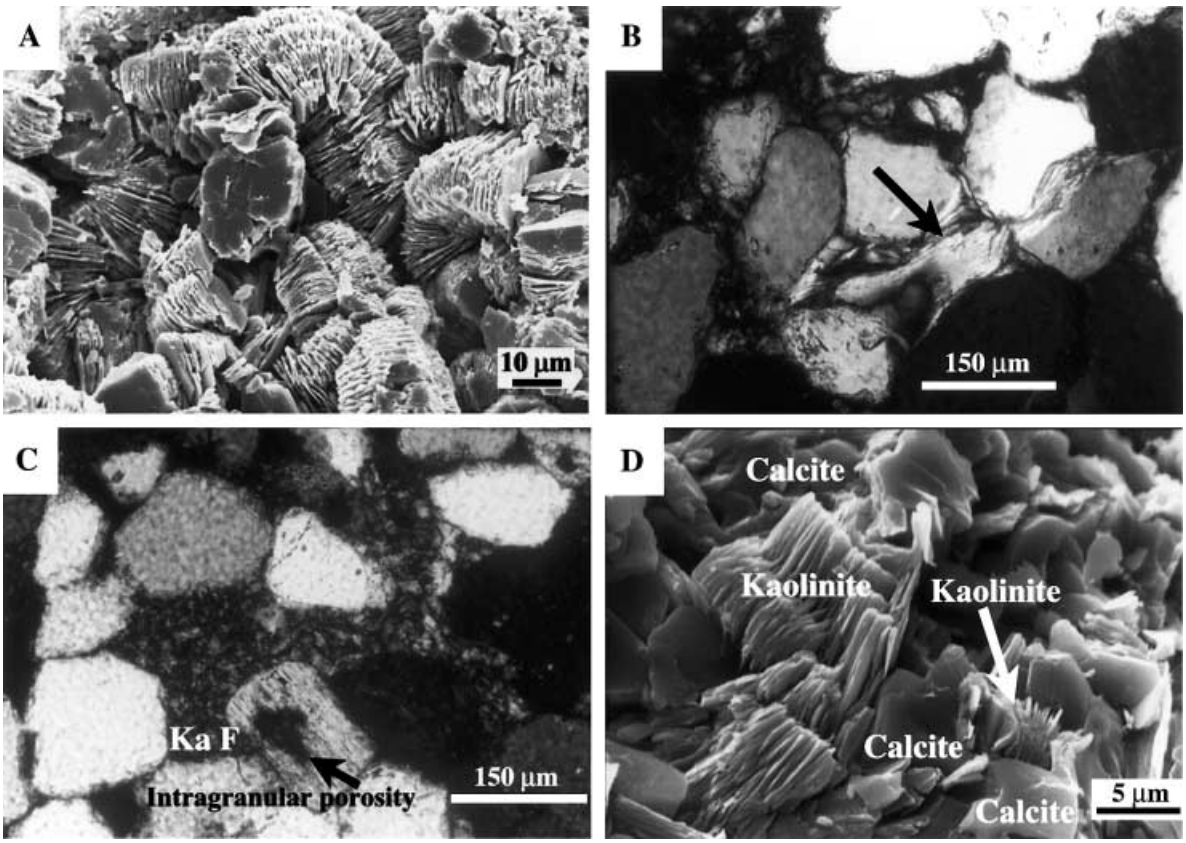

Fig. 10. (A) SEM image showing kaolinite as booklets and vermicular aggregates composed of several platelets. (B) Photomicrograph (crossed nicols) showing mica with expanded texture into large open pores (arrow). (C) Photomicrograph (crossed nicols) showing collapsed kaolinitized feldspars (Ka F) and intragranular porosity in feldspar grains. (D) SEM image showing calcite engulfing vermicular kaolinite aggregates.

Quartz

Quartz cement occurs as euhedral, syntaxial overgrowths around detrital quartz grains. Diagenetic quartz occurs as a minor constituent in sandstones of all systems tracts (Table S1), and shows no obvious distribution pattern related to facies or sequence stratigraphy. Quartz overgrowths engulf, and thus post-date, kaolinite, chlorite and framboidal pyrite, but are engulfed and covered by, and thus predate, ankerite.

Feldspars

Diagenetic feldspars are minor constituents in sandstones of all systems tracts (Table S1) and occur as thin (10–20 μm) K-feldspar and albite overgrowths around detrital feldspar grains and as small (40 μm) prismatic crystals replacing detrital plagioclase grains. Diagenetic feldspars show no obvious distribution pattern in relation to facies or sequence stratigraphy.

Other diagenetic minerals

Other diagenetic minerals occur as traces and include Ti-oxides, anhydrite and apatite (Table S1). Ti-oxides occur as small (5–10 μm) euhedral anatase crystals that form aggregates around altered biotite and sphene grains. Anatase crystals are engulfed by, and thus predate, quartz overgrowths and calcite. Anatase shows no obvious distribution pattern with facies or sequence stratigraphy. Anhydrite occurs as small (< 10 μm) crystals that are closely associated with microcrystalline pyrite, and are engulfed by, and thus post-date, blocky pyrite and calcite. Apatite occurs as polycrystalline aggregates that fill pores within carbonate bioclasts, being closely associated with siderite in bioclastic lags at parasequence boundaries of the upper sequence.

POROSITY

Thin-section porosity of the sandstones includes intergranular and intragranular macropores formed by the dissolution of lithic fragments and feldspars (Fig. 10C). Microporosity is revealed by SEM examination to occur in pseudomatrix, kaolinite, chlorite aggregates, albitized feldspars and expanded and kaolinitized micas. The average intergranular and total thin-section porosity is fairly similar for the LST deltaic (7% and 11% respectively), TST estuarine (8% and 9% respectively) and for the TST foreshore and shoreface sandstones (9%; Table S1). Lag deposits associated with transgressive surfaces, sequence and parasequence boundaries have very low total and intergranular porosities (averages < 1%; Table S1). Intragranular porosity is higher in the LST deltaic sandstones (average 4%) than in the TST estuarine (average 2%) and in the TST and HST foreshore and shoreface (average < 1%) sandstones (Table S1). Lag deposits at transgressive surfaces, sequence and parasequence boundaries have very low intragranular porosity (averages < 1%; Table S1).

Variations in sandstone porosity occur within parasequences of the TST. Sandstone beds 0–3 m above coal-bearing parasequence boundaries have low porosity (< 1%; Fig. 7). Sandstones in the upper part of parasequences with no coal layers have porosity values > 10% (Fig. 7). The most porous sandstones (porosity > 10%) occur in the middle part of parasequences between the two low-porosity zones at the upper and lower parasequence boundaries (Fig. 7). This pattern of porosity distribution can be detected in the resistivity logs. High resistivity values (e.g. 500 ohm-m) correspond to low-porosity sandstones (< 1%) at the base of parasequences, whereas low resistivity values (e.g. 300 ohm-m) correspond to more porous sandstones in the middle and top of parasequences (Fig. 7).

DISCUSSION

Diagenetic alterations such as grain dissolution and cementation by pyrite, calcite, siderite and kaolinite display systematic spatial distribution patterns within the sequence stratigraphic framework of the Rio Bonito Formation. Conversely, ankerite, chlorite, feldspar and quartz cements show no obvious distribution pattern within the sequence stratigraphic framework.

Diagenetic alterations associated with LST and sequence boundary

The dissolution of framework grains and formation of kaolinite in the LST alluvial and deltaic sandstones of the lower sequence has possibly occurred during near-surface eodiagenesis, i.e. before significant compaction, as indicated by the expanded texture of kaolinitized micas and the collapsed texture of extensive kaolinitized feldspar grains. These sandstones are more prone to kaolinitization and grain dissolution compared with the TST and

HST estuarine, foreshore and shoreface facies, because of more effective exposure to meteoric water circulation during near-surface diagenesis (Morad *et al.*, 2000). The humid climatic conditions that prevailed during deposition enhanced meteoric water percolation and dissolution of feldspars, micas and lithic fragments, and the formation of kaolinite (Ketzer *et al.*, 2003).

In addition to the formation of kaolinite in the LST deposits of the lower sequence, local increase in kaolinite content in the lag deposit of the upper sequence and below the upper sequence boundary is attributed to possible subaerial exposure of the shelf during fall in relative sea level (regression) and meteoric water flushing of marine sediments (Morad *et al.*, 2000; Ketzer *et al.*, 2003).

Diagenetic alterations associated with TST, HST, transgressive surface and maximum flooding surface

The formation of pyrite, calcite, siderite and kaolinite, and grain dissolution, occurred mainly in sandstones of the TST and HST in the vicinity of parasequence boundaries, transgressive surface and maximum flooding surface.

Grain dissolution and kaolinite formation

Grain dissolution and kaolinite formation below parasequence boundaries with coal deposits (i.e. in the TST) occurred at shallow burial depths, before significant burial (Fig. 11), by meteoric waters charged with CO_2 and organic acids as a

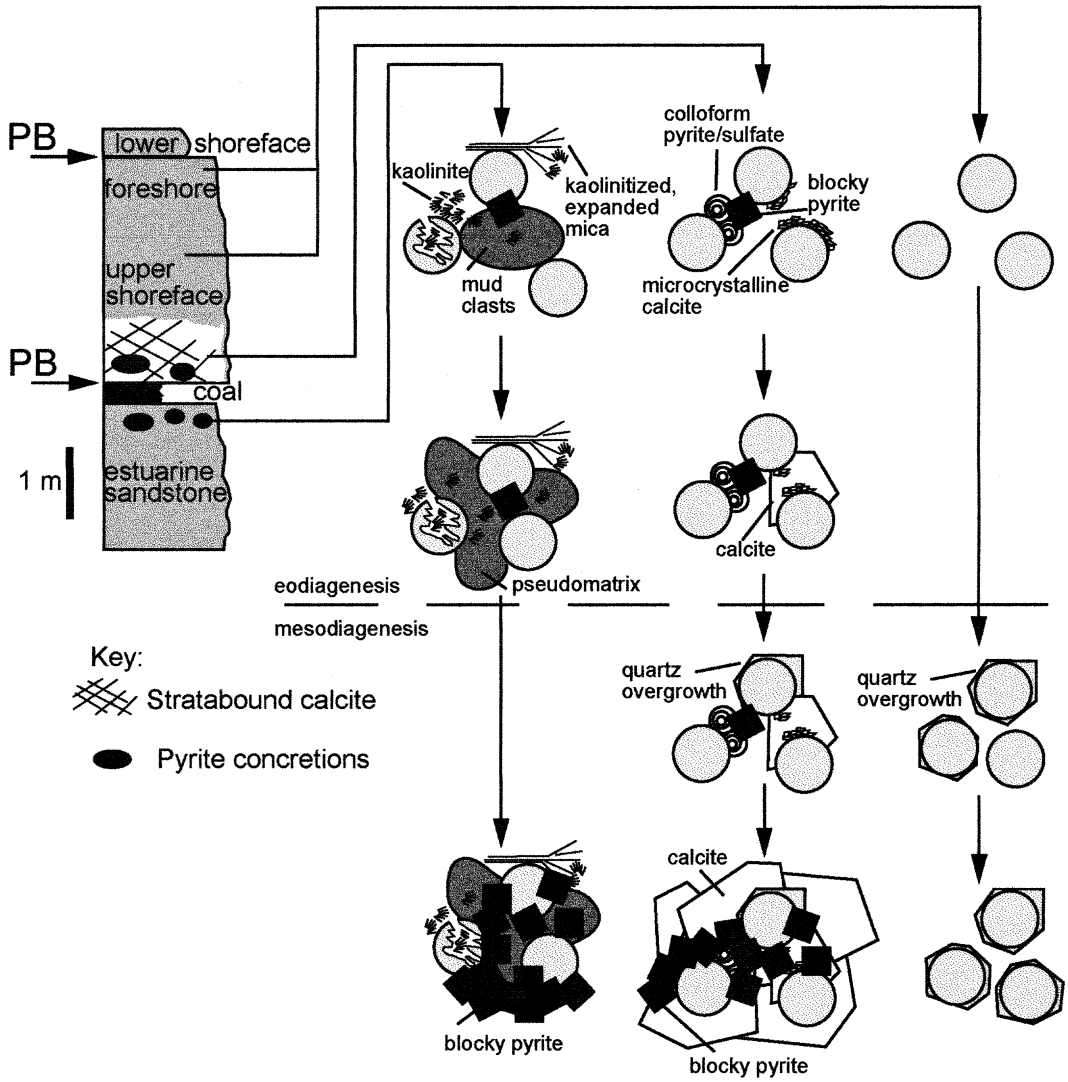

Fig. 11. Diagram showing the main pore-filling sequence of TST estuarine, shoreface and foreshore sandstones of the lower sequence. Note that cementation by pyrite and calcite was focused in sandstones in the vicinity of parasequence boundaries (PB).

result of percolation through peat deposits (Staub & Cohen, 1978). Nevertheless, organic acids and CO_2 can also be formed during thermal alteration of organic matter (Surdam *et al.*, 1984; Van Keer *et al.*, 1998), and may thus have contributed to grain dissolution and kaolinite formation during mesodiagenesis.

In contrast to kaolinite, the restricted occurrence of chlorite to one TST shoreface sandstone sample and one lag deposit at a sequence boundary precludes its systematic distribution pattern in a sequence stratigraphic framework. Chlorite formation in such sediments is usually attributed to mesogenetic transformation of iron-rich, clay precursors such as berthierine and odinite, which are common eogenetic minerals in paralic and shallow-marine settings (Odin & Matter, 1981; Ehrenberg, 1993).

Pyrite

Extensive pyrite cementation in the TST sandstones, below and above parasequence boundaries with coal layers, occurred in two stages. The first stage resulted in the formation of microcrystalline pyrite associated with gypsum/anhydrite (Fig. 11). During transgression and formation of the parasequence boundaries, sulphate dissolved in sea water, which invaded the coastal sand deposits, was reduced to sulphide during bacterial alteration of organic matter in the peat deposits and formed microcrystalline pyrite. Continuous flux of sea water during transgression may have resulted in alternating reducing and oxidizing conditions, and hence the precipitation of microcrystalline pyrite and gypsum/anhydrite in the shoreface sandstones overlying peat deposits. Small amounts of grain-rimming microcrystalline calcite were probably formed during this initial stage of pyrite cementation. The timing of blocky, concretionary pyrite cementation of sandstones above and below parasequence boundaries with coal layers, which occurred by nucleation on framboidal pyrite and colloform pyrite/anhydrite aggregates, is poorly constrained (Fig. 11). Changes in pyrite texture, from microcrystalline to blocky, suggest a progressive restriction in the supply of sea water (Raiswell, 1987).

Calcite and ankerite

Calcite in the Rio Bonito Formation occurs mainly as stratabound cement along parasequence boundaries. Such a distribution pattern of calcite cementation at parasequence boundaries is usually attributed to the increased amount of carbonate bioclasts (South and Talbot, 2000; Ketzer *et al.*, 2002) and/or to the long residence time of the sediments at shallow depths below the sea floor (Taylor *et al.*, 1995). The precipitation of Fe-poor calcite (Table 2) concomitantly with pyrite concretions in the Rio Bonito sandstones lying above parasequence boundaries with the coal layer, however, was probably aided by an increase in carbonate alkalinity resulting from bacterial sulphate reduction in the coal (Curtis, 1987).

The relationship between calcite and other diagenetic minerals indicates that cementation commenced at near sea floor conditions, with microcrystalline texture, and continued as mosaic and poikilotopic crystals during shallow burial (i.e. eodiagenesis) and later during mesodiagenesis (Fig. 11). Distinction between these two phases of cementation (i.e. eo- and mesodiagenesis) is not straightforward, because both calcites display a similar texture and blotchy cathodoluminescence pattern. Mesogenetic calcite has presumably nucleated on earlier microcrystalline calcite and on eogenetic poikilotopic calcite above parasequence boundaries with coal layers, which is evidenced by the intimate occurrence of all three types of calcite. A similar pattern of carbonate cementation associated with parasequence boundaries occurs in the Upper Cretaceous sandstones of the Book Cliffs, USA (Taylor *et al.*, 1995, 2000). TST sandstones that are devoid of eogenetic calcite cement contain only small quantities of mesogenetic calcite and are, instead, cemented by quartz (Fig. 11).

The fairly low $\delta^{13}C_{VPDB}$ values of calcite cement (between −7·7‰ and −3·6‰) suggest that carbon was derived mainly from alteration of organic matter, most likely C_3 and C_4 plant remains ($\delta^{13}C$ values of dissolved carbon ≈ −14‰ and −2‰ respectively; Morad, 1998) in the peat/coal deposits. However, the input of dissolved carbon from sea water and from the alteration of marine organic matter cannot be excluded. The $\delta^{18}O_{VPDB}$ values show a wide range (−16·7‰ and −8·2‰), which partly reflects the presence of different proportions of eogenetic and mesogenetic calcites in these samples. If we use these $\delta^{18}O_{VPDB}$ values in the fractionation equation of Friedman and O'Neil (1977) and assume a $\delta^{18}O_{VSMOW}$ value of −1‰ for the porewater, which is equivalent to moderately evolved formation water relative to the contemporary early Permian sea water (−3‰; Veizer *et al.*, 1997), calcite would have precipitated at temperatures between 52 °C and 124 °C.

These temperatures are compatible with calcite formation during early and deep burial. The highest temperature obtained for calcite precipitation (124 °C) agrees with the maximum temperature reached by the Rio Bonito Formation, as indicated by the vitrinite reflectance values ($R_0 = 0{\cdot}56$; Holz *et al.*, 2002).

The $\delta^{18}O_{VPDB}$ values of ankerite, which predates mesogenetic calcite, show a wide range (−12·5‰ to −7·5‰). If these $\delta^{18}O_{VPDB}$ values are used in the fractionation equation of Fisher and Land (1986) and the same formation water values are used as is assumed for calcite (i.e. $\delta^{18}O_{VSMOW}$ −1‰), ankerite would have precipitated at temperatures between 67 °C and 110 °C. This temperature range agrees well with typical temperatures for the formation of mesogenetic ankerite (Spötl & Pitman, 1998). The $\delta^{13}C_{VPDB}$ values of ankerite (−4·7‰ to −3·3‰) are not diagnostic of the diagenetic conditions, other than suggesting that carbon was derived from the alteration of organic matter.

Siderite

The close association of siderite cement, which is restricted to lags of TST parasequence boundaries and the TS of the upper sequence, with apatite suggests that iron reduction possibly occurred in suboxic conditions close to the sediment–water interface (Berner, 1981; Mozley & Carothers, 1992; Morad, 1998). Prolonged suboxic conditions in marine sediments, which are facilitated during low sedimentation rates (Raiswell, 1987; Gaynor & Scheihing, 1988; Chow *et al.*, 2000) at parasequence boundaries and transgressive surface (Posamentier & Allen, 1999), therefore facilitated siderite formation.

The single values for $\delta^{13}C_{VPDB}$ (−5·1‰) and $\delta^{18}O_{VPDB}$ (−12·2‰) of siderite preclude a precise constraining of its origin. The $\delta^{13}C_{VPDB}$ value is typical for porewaters in which dissolved carbon is derived from alteration of organic matter under suboxic conditions (McArthur *et al.*, 1986). The negative $\delta^{18}O_{VPDB}$ value is incompatible with low-temperature precipitation of siderites in marine sediments. Examination of $\delta^{18}O$ values of siderites available in the literature (Hart *et al.*, 1992; Mozley & Carothers, 1992; Huggett *et al.*, 2000), however, revealed that such ^{18}O depletion is common for early diagenetic siderites in such environments. A plausible explanation is the oxygen isotopic fractionation by microbial organisms during the formation of siderite in marine sediments, which results in $\delta^{18}O$ values considerably lower than sea water (Mortimer & Coleman, 1997).

Porosity evolution and prediction in a sequence stratigraphic framework

The depositional facies-related porosity of sandstones was modified considerably during diagenesis owing to cementation by pyrite, calcite, siderite and kaolinite, dissolution of framework grains and compaction. Moreover, diagenesis also created reservoir compartments. A plot of sandstone intergranular volume vs. cement volume indicates that compaction was more important than cementation in destroying primary porosity (Fig. 12). Eogenetic cements (e.g. calcite, pyrite and siderite) have pervasively destroyed the depositional porosity of sandstones lying in the vicinity of parasequence boundaries in the TST of the lower sequence, of sandstones lying along the sequence boundary and of the transgressive surface lag deposits of the upper sequence.

Porosity distribution is predictable in sandstones of the TST and HST parasequence of the lower sequence. Sandstones located 0–3 m above the lower parasequence boundary containing a coal layer have very low porosity (< 1%) because of extensive pyrite and calcite cementation. The association of extensive stratabound calcite cementation (i.e. low porosity) sandstones with parasequence boundaries having coal layers can be identified in wireline logs by their high resistivity values (Fig. 7). Such high resistivity values are not encountered in the porous middle part of parasequences (Fig. 7). Coal layers do not occur in the distal parts of parasequence boundaries of the upper TST in which the boundary is marked by lower shoreface sandstones overlying the upper shoreface sandstone. The latter sandstones are poorly cemented and comprise the most porous rocks in the studied interval. In more proximal areas, however, where parasequences contain a coal layer at their tops, sandstone porosity is partly destroyed by concretionary pyrite cementation in the first 50 cm below the coal layer. Intragranular porosity may, in this case, be locally enhanced by up to 5%. Grain dissolution and formation of intragranular porosity (up to 7%) also occurred in sandstones of the LST in the lower sequence (deltaic sandstones). In this latter case, the generation of intragranular porosity was not, however, focused along parasequence boundaries, and no vertical trends in porosity variation can be detected.

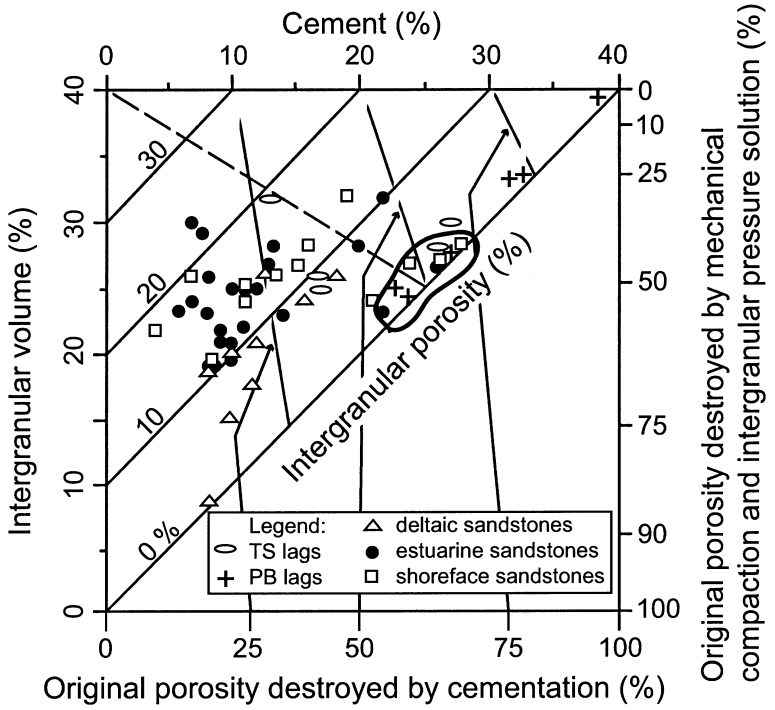

Fig. 12. Plot of intergranular volume (IGV) vs. volume of cement (Houseknecht, 1988; modified by Ehrenberg, 1989) of 56 representative sandstone samples. LST, TST and HST refer to lowstand, transgressive and highstand systems tracts respectively. Note that cementation was more important in destroying original porosity in lag deposits and in sandstone samples located in the vicinity of parasequence boundaries of the TST of the lower sequence (marked area).

General model for the distribution of diagenetic alterations in a sequence stratigraphic framework

A general model for the distribution of diagenetic alteration in the Rio Bonito Formation reflects the sequence stratigraphic distribution of coal layers as well as changes in porewater chemistry related to changes in relative sea level. Earlier studies have revealed that the sequence stratigraphic distribution of diagenetic alterations (e.g. calcite, dolomite, siderite, kaolinite, grain dissolution) in siliciclastic deposits is usually linked to sequence and parasequence boundaries (Taylor *et al.*, 1995, 2000; South & Talbot, 2000; Ketzer *et al.*, 2002, 2003). Such stratigraphic surfaces are the locus of carbonate cementation owing to the presence of carbonate bioclasts and the long residence time of sediments at shallow depths below the sea floor. The latter is important in the Rio Bonito Formation for the formation of siderite in carbonate bioclast lags, which occur at parasequence boundaries (Fig. 13). The parasequence boundaries may have coal layers instead of carbonate bioclast lags. Diagenesis of organic matter in these coal layers promoted the formation of stratabound calcite and concretionary pyrite along these surfaces (Fig. 13). Parasequence boundaries with coal layers are thus additional potential sites for carbonate cementation. As calcite and pyrite cements are spatially related to coal layers at parasequence boundaries, they are spatially distributed according to the retrogradational pattern of the TST parasequences, and the progradational pattern of the HST parasequences (Fig. 13). These diagenetic alterations do not occur in basinward extensions of parasequence boundaries because of the basinward absence of coal layers (Fig. 13). This conceptual model for the distribution of diagenetic alterations and related porosity evolution in coal-bearing sandstone deposits allows the prediction of possible baffles for vertical fluid flow and reservoir compartments at TST and HST parasequences boundaries, transgressive surfaces and maximum flooding surfaces (Fig. 13).

Despite carbonate cementation, sandstones below sequence and parasequence boundaries may contain kaolinite and grain dissolution, mainly owing to meteoric water percolation (Ketzer *et al.*, 2003). In the Rio Bonito Formation, kaolinite and grain dissolution are related to meteoric water infiltration related to both subaerial exposure of the parasequence boundaries and the basinward shift in the meteoric water zone. The increase in the amounts of kaolinite and grain dissolution below parasequence boundaries with coal layers is attributed here to the generation of organic acids and CO_2 during percolation of meteoric waters in the peat deposits (Fig. 13).

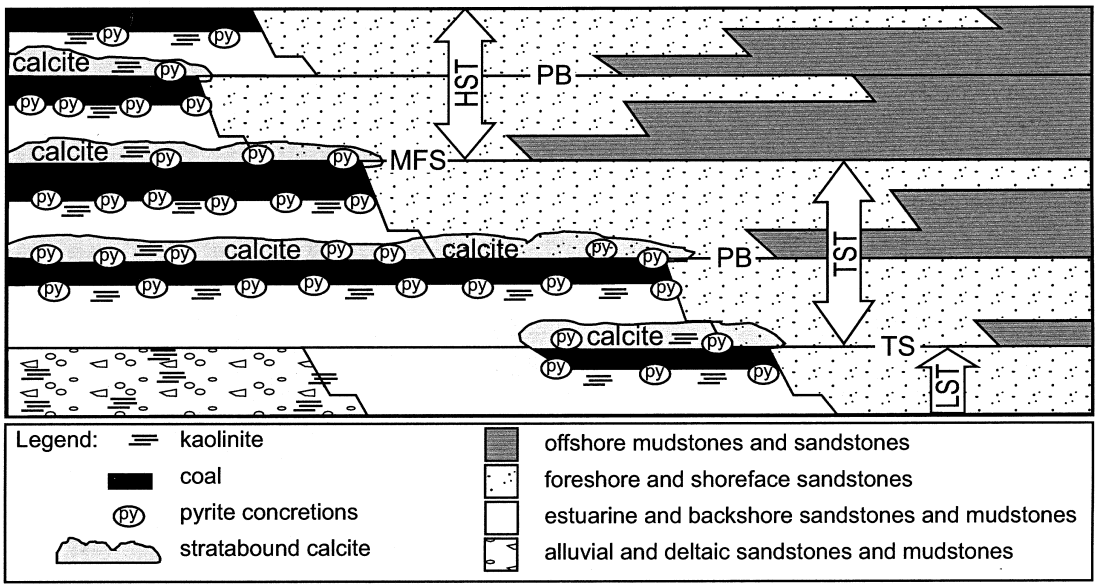

Fig. 13. A cartoon illustrating the spatial distribution of pyrite concretions, stratabound calcite and kaolinite for the lower sequence in the context of sequence stratigraphy. Note that cementation is spatially related to the coal layers, which follow the retrogradational and progradational stacking patterns of the TST and HST respectively. Stratabound calcite at parasequence boundaries potentially forms baffles for vertical fluid flow and reservoir compartments.

CONCLUSIONS

This paper demonstrates that sequence stratigraphy can provide important information about parameters (porewater chemistry, detrital composition, residence time and amounts of organic matter) controlling the formation and distribution pattern of diagenetic alterations and related reservoir quality evolution in paralic, coal-bearing siliciclastic deposits. Diagenetic alterations in the Rio Bonito Formation (early Permian) that are linked to sequence stratigraphy include cementation by calcite, pyrite, kaolinite and siderite, and dissolution of framework grains, whereas those not related to sequence stratigraphy include cementation by quartz, feldspars, ankerite and chlorite.

Parasequence boundaries are common places for extensive cementation during eo- and mesodiagenesis, and thus for porosity destruction. The sequence stratigraphic distribution of coal layers, which occur at the top of parasequences within TST and upper LST, has a profound impact on the distribution of calcite, pyrite and kaolinite cements, and on grain dissolution. Diagenesis of coal resulted in extensive sulphate reduction and the formation of concretionary pyrite in sandstones below and above parasequence boundaries. Diagenesis of coal also resulted in an increase in carbonate alkalinity, and hence the formation of stratabound calcite in estuarine and shallow-marine sandstones located immediately above (0–3 m) parasequence boundaries. Such stratabound calcite cementation, which follows the backstepping pattern of the coal layers, is recognizable in resistivity logs and implies that reservoir compartments can be formed in sandstones in the vicinity of parasequence boundaries with coal layers.

Meteoric water percolation through peat deposits enhanced the dissolution of silicate grains and the formation of kaolinite in sandstones below parasequence boundaries. Formation of concretionary pyrite, kaolinite and grain dissolution occurred below coal layers at parasequence boundaries too, and resulted in a net loss of porosity. Formation of kaolinite and grain dissolution also occurred in marine sandstone below sequence boundaries owing to the basinward shift in the meteoric water zone during relative sea-level fall.

Eogenetic cementation by siderite (and traces of apatite) occurred mainly in shallow-marine, LST sandstones and bioclastic lag deposits at the transgressive surface and parasequence boundaries, mainly as a result of the prolonged residence time of the sediments on the sea floor and balanced organic matter content, which sustained suboxic conditions. Siderite cementation

resulted in deterioration of porosity and, thus, siderite-cemented bioclastic lag deposits at the transgressive surface and parasequence boundaries are potential sites for the formation of reservoir compartments between the LST and TST sandstones and sandstones of adjacent parasequences.

This study shows that a predictable, conceptual model for the distribution of diagenetic alteration and fluid flow baffles in coal-bearing sequences is possible by integrating diagenesis and sequence stratigraphy. This case study serves as an analogue for coal-bed methane and other coal-bearing reservoir studies.

ACKNOWLEDGEMENTS

J. M. Ketzer thanks the Brazilian National Research Council (CNPq – grant no. 200059/98-0) and the Geologiska sektionen at Uppsala University (Otterborgs donationfond 2001) for financial support. M. Holz acknowledges CNPq for research and study grants (no. 352887/96-6). I. S. Al-Aasm thanks the Natural Sciences and Engineering Research Council of Canada (NSERC). The authors thank both the Companhia Riograndense de Mineração (CRM) and the Companhia de Pesquisas de Recursos Minerais (CPRM) for allowing access to the well logs, cores, rock samples and to the Candiota Coal Mine. We also thank Hans Harryson for aiding with the microprobe analysis, Risto Kumpulainen at Stockholm University for helping with the cathodoluminescence analysis, and students at Universidade Federal do Rio Grande do Sul (Brazil), Juliano Küchle, Alan Bischof and Naoki Arima for assistance during fieldwork. Roberto Carlucci is acknowledged for discussions about the sequence stratigraphic framework of the Rio Bonito Formation. We acknowledge Stephen Ehrenberg, R. Gaupp and an anonymous reviewer, Alastair Ruffell and Christoph Spötl for providing us with valuable comments and suggestions.

SUPPLEMENTARY MATERIAL

The following material is available from http://www.blackwellpublishing.com/products/journals/suppmat/sed/sed586/sed586sm.htm

Table S1. Modal composition (maximum, minimum, average and standard deviation) of sandstone samples of the Rio Bonito Formation.

REFERENCES

Al-Aasm, I.S., Taylor, B.E. and **South, B.** (1990) Stable isotope analysis of multiple carbonate samples using selective acid extraction. *Chem. Geol.*, **80,** 119–125.

Alves, R.G. and **Ade, M.V.B.** (1996) Sequence stratigraphy and organic petrography applied to the study of Candiota Coal Field, RS, South Brazil. *Int. J. Coal Geol.*, **30,** 231–248.

Amorosi, A. (1995) Glaucony and sequence stratigraphy: conceptual framework of distribution in siliciclastic sequences. *J. Sed. Res.*, **B65,** 419–425.

Amorosi, A. (1997) Detecting compositional, spatial, and temporal attributes of glaucony: a tool for provenance research. *Sed. Geol.*, **109,** 135–153.

Amorosi, A. and **Centineo, M.C.** (2000) Anatomy of a condensed section: the Lower Cenomanian glaucony-rich deposits of Cap Blanc-Nez (Boulonnais, northern France). In: *Marine Authigenesis: from Global to Microbial* (Eds C.R. Glenn, J. Lucas and L. Lucas), *SEPM Spec. Publ.*, **66,** 405–413.

Berner, R.A. (1981) A new geochemical classification of sedimentary environments. *J. Sed. Petrol.*, **51,** 359–365.

Bustin, R.M., Hill, L.V. and **Gunther, P.R.** (1977) Implications of coalification levels, Eureka Sound Formation, northeastern Arctic Canada. *Can. J. Earth Sci.*, **14,** 1588–1597.

Chow, N., Morad, S. and **Al-Aasm, I.** (2000) Origin of authigenic Mn-Fe carbonates and pore-water evolution in marine sediments: evidence from Cenozoic strata of the Artic Ocean and Norwegian-Greenland Sea (ODP Leg 151). *J. Sed. Res.*, **70,** 682–699.

Curtis, C.D. (1987) Inorganic geochemistry and petroleum exploration. In: *Advances in Petroleum Geochemistry*, Vol. 2 (Eds J. Brooks and D. Welte), pp. 91–140. Academic Press, London.

Curtis, C.D. and **Coleman, M.L.** (1986) Controls on the precipitation of early diagenetic calcite, dolomite and siderite concretions in complex depositional sequences. In: *Roles of Organic Matter in Sediment Diagenesis* (Ed. D.L. Gautier), *SEPM Spec. Publ.*, **38,** 23–33.

Daemon, R.F. and **Marques-Toigo, M.** (1991) An interpreted biostratigraphic column for the Paraná Basin, Brazil. *International Congress on Carboniferous–Permian Geology and Stratigraphy*, Buenos Aires, Argentina, p. 25.

Dutton, S.P. and **Willis, B.J.** (1998) Comparison of outcrop and subsurface sandstone permeability distribution, Lower Cretaceous Fall River Formation, South Dakota and Wyoming. *J. Sed. Res.*, **A68,** 890–900.

Ehrenberg, S.N. (1989) Assessing the relative importance of compaction processes and cementation to reduction of porosity in sandstones: discussion; Compaction and porosity evolution of Pliocene sandstones, Ventura Basin, California: discussion. *AAPG Bull.*, **73,** 1274–1276.

Ehrenberg, S.N. (1993) Preservation of anomalously high porosity in deeply buried sandstones by grain-coating chlorite: examples from the Norwegian continental shelf. *AAPG Bull.*, **77,** 1260–1286.

Fisher, R.S. and **Land, L.S.** (1986) Diagenetic history of Eocene Wilcox sandstones, south-central Texas. *Geochim. Cosmochim. Acta*, **50,** 551–561.

Friedman, I. and **O'Neil, J.R.** (1977) Compilation of stable isotopic fractionation factors of geochemical interest. *US Geol. Surv. Prof. Paper*, **440-KK,** 12 pp.

Gaynor, G.C. and **Scheihing, M.H.** (1988) Shelf depositional environments and reservoir characteristics of the Kuparuk River Formation (Lower Cretaceous), Kuparuk Field, North

Slope, Alaska. In: *Giant Oil and Gas Fields: a Core Workshop* (Eds A.J. Lomando and P.M. Harris), *SEPM Core Workshop*, **12,** 333–389.

Hart, B.S., Longstaffe, F.J. and **Plint, A.G.** (1992) Evidence for relative sea-level changes from isotopic and elemental composition of siderite in the Cardium Formation, Rocky Mountain Foothills. *Bull. Can. Petrol. Geol.*, **40,** 52–59.

Holz, M. (1999) Early Permian sequence stratigraphy and the palaeophysiographic evolution of the Paraná Basin in southernmost Brazil. *J. South Afr. Earth Sci.*, **29,** 51–61.

Holz, M., Kalkreuth, W. and **Banerjee, I.** (2002) Sequence stratigraphy of paralic coal-bearing strata: an overview. *Int. J. Coal Geol.*, **48,** 147–179.

Houseknecht, D.W. (1988) Intergranular pressure solution in four quartzose sandstones. *J. Sed. Petrol.*, **58,** 228–246.

Huggett, J., Dennis, P. and **Gale, A.** (2000) Geochemistry of early siderite cements from the Eocene succession of Whitecliff Bay, Hampshire Basin, UK. *J. Sed. Res.*, **70,** 1107–1117.

Iijima, A. and **Matsumoto, S.R.** (1982) Berthierine and chamosite in coal measures of Japan. *Clay Clay Mineral.*, **30,** 264–274.

Kantorowicz, J.D., Bryant, I.D. and **Dawans, J.M.** (1987) Controls on the geometry and distribution of carbonate cements in Jurassic sandstones: Bridport Sands, southern England and Viking Group, Troll Field, Norway. In: *Diagenesis of Sedimentary Sequences* (Ed. J.D. Marshall), *Geol. Soc. London Spec. Publ.*, 36, 103–118.

Ketzer, J.M., Morad, S., Evans, R. and **Al-Aasm, I.S.** (2002) Distribution of diagenetic alterations in fluvial, deltaic, and shallow marine sandstones within a sequence stratigraphic framework: evidence from the Mullaghmore Formation (Carboniferous), NW Ireland. *J. Sed. Res.*, **72,** 760–774.

Ketzer, J.M., Morad, S. and **Amorosi, A.** (2003) Predictive diagenetic clay-mineral distribution in siliciclastic rocks within a sequence stratigraphic framework. In: *Clay Mineral Cements in Sandstones* (Eds R. Worden and S. Morad), *Int. Assoc. Sedimentol. Spec. Publ.*, **34,** 42–59.

Klein, J.S., Mozley, P., Campbell, A. and **Cole, R.** (1999) Spatial distribution of carbon and oxygen isotopes in laterally extensive carbonate-cemented layers: implications for mode of growth and subsurface identification. *J. Sed. Res.*, **69,** 184–191.

Loomis, J.L. and **Crossey, L.J.** (1996) Diagenesis in a cyclic, regressive siliciclastic sequence: the Point Lookout Sandstone, San Juan Basin, Colorado. In: *Siliciclastic Diagenesis and Fluid Flow: Concepts and Applications* (Eds L.J. Crossey, R. Loucks and M.W. Totten), *SEPM Spec. Publ.*, **55,** 23–36.

McArthur, J.M., Benmore, R.A., Coleman, M.L., Soldi, C., Yeh, H.W. and **O'Brien, G.W.** (1986) Stable isotopic characterization of francolite formation. *Earth Planet. Sci. Lett.*, **77,** 20–34.

McBride, E.F. (1963) A classification of common sandstones. *J. Sed. Petrol.*, **33,** 664–669.

McKay, J.L., Longstaffe, F.J. and **Plint, A.G.** (1995) Early diagenesis and its relationship to depositional environment and relative sea-level fluctuations (Upper Cretaceous Marshybank Formation, Alberta and British Columbia). *Sedimentology*, **42,** 161–190.

Matsumoto, R. and **Iijima, A.** (1981) Origin and diagenetic evolution of Ca-Mg-Fe carbonates in some coalfields of Japan. *Sedimentology*, **28,** 239–259.

Morad, S. (1998) Carbonate cementation in sandstones: distribution patterns and geochemical evolution. In: *Carbonate Cementation in Sandstones* (Ed. S. Morad), *Int. Assoc. Sedimentol. Spec. Publ.*, **26,** 1–26.

Morad, S., Marfil, R., Al-Aasm, I.S. and **Gomez-Gras, D.** (1992) The role of mixing-zone dolomitization in sandstone cementation: evidence from the Triassic Buntsandstein, the Iberian Range, Spain. *Sed. Geol.*, **80,** 53–65.

Morad, S., Ketzer, J.M. and **De Ros, L.F.** (2000) Spatial and temporal distribution of diagenetic alterations in siliciclastic rocks: implications for mass transfer in sedimentary basins. *Sedimentology*, **47** (Suppl. 1), 95–120.

Mortimer, R.J.G. and **Coleman, M.L.** (1997) Microbial influence of the oxygen isotopic composition of diagenetic siderite. *Geochim. Cosmochim. Acta*, **6,** 1705–1711.

Moss, S.J. and **Tucker, M.E.** (1996) Dolomitization associated with transgressive surfaces – a mid-Cretaceous example. *Sed. Geol.*, **107,** 11–20.

Mozley, P.S. and **Carothers, W.W.** (1992) Elemental and isotopic composition of siderite in the Kuparuk Formation, Alaska: effect of microbial activity and water/sediment interaction on early pore-water chemistry. *J. Sed. Petrol.*, **62,** 681–692.

Odin, G.S. and **Matter, A.** (1981) De glauconiarum origine. *Sedimentology*, **28,** 611–641.

Patzkowsky, M.E., Smith, L.H., Markwick, P.J., Engberts, C.J. and **Gyllenhaal, E.D.** (1991) Application of the Fuijita-Ziegler paleoclimatic model: early Permian and late Cretaceous examples. *Palaeogeogr., Palaeoclimatol., Palaeoecol.*, **86,** 67–85.

Posamentier, H.W. and **Allen, G.P.** (1999) *Siliciclastic Sequence Stratigraphy – Concepts and Applications*. SEPM Concepts in Sedimentology and Paleontology 7. SEPM, Tulsa, 210 pp.

Raiswell, R. (1987) Non-steady state microbiological diagenesis and the origin of concretions and nodular limestones. In: *Diagenesis of Sedimentary Sequences* (Ed. J.D. Marshall), *Geol. Soc. London Spec. Publ.*, **36,** 41–54.

Read, J.F. and **Horbury, A.D.** (1993) Eustatic and tectonic controls on porosity evolution beneath sequence-bounding unconformities and parasequences disconformities on carbonate platforms. In: *Diagenesis and Basin Development* (Eds A.D. Horbury and A.G. Robinson), *AAPG Stud. Geol.*, **36,** 155–197.

Smith, A.G., Hurley, A.M. and **Briden, J.C.** (1981) *Phanerozoic Palaeocontinental World Maps*. Cambridge University Press, Cambridge, 102 pp.

South, D.L. and **Talbot, M.R.** (2000) The sequence stratigraphic framework of carbonate diagenesis within transgressive fan-delta deposits: Sant Llorenç del Munt fan-delta complex, SE Ebro Basin, NE Spain. *Sed. Geol.*, **138,** 179–198.

Spötl, C. and **Pitman, J.K.** (1998) Saddle (baroque) dolomite in carbonates and sandstones: a reappraisal of a burial-diagenetic concept. In: *Carbonate Cementation in Sandstones* (Ed. S. Morad), *Int. Assoc. Sedimentol. Spec. Publ.*, **26,** 437–460.

Staub, J.R. and **Cohen, A.D.** (1978) Kaolinite-enrichment beneath coals: a modern analog, Snuggedy swamp, South Carolina. *J. Sed. Petrol.*, **48,** 203–210.

Surdam, R.C., Boese, S.W. and **Crossey, L.J.** (1984) The chemistry of secondary porosity. In: *Clastic Diagenesis* (Eds D.A. McDonald and R.C. Surdam), *AAPG Mem.*, **37,** 127–149.

Tang, Z., Parnell, J.P. and **Ruffell, A.H.** (1994) Deposition and diagenesis of the lacustrine-fluvial Cangfanggou Group (uppermost Permian to Lower Triassic), southern Junggar

Basin, NW China: a contribution from sequence stratigraphy. *J. Paleolimnol.*, **11,** 67–90.

Taylor, K.G. and **MacQuaker, J.H.S.** (2000) Spatial and temporal distribution of authigenic minerals in continental shelf sediments: implications for sequence stratigraphic analysis. In: *Marine Authigenesis: from Global to Microbial* (Eds C.R. Glenn, J. Lucas and L. Lucas), *SEPM Spec. Publ.*, **66,** 309–323.

Taylor, K.G., Gawthorpe, R.L. and **Van Wagoner, J.C.** (1995) Stratigraphic control on laterally persistent cementation, Book Cliff, Utah. *J. Sed. Res.*, **69,** 225–228.

Taylor, K.G., Gawthorpe, R.L., Curtis, C.D., Marshall, J.D. and **Awwiller, D.N.** (2000) Carbonate cementation in a sequence stratigraphic framework: Upper Cretaceous sandstones, Book Cliffs, Utah–Colorado. *J. Sed. Res.*, **70,** 360–372.

Tucker, M.E. (1993) Carbonate diagenesis and sequence stratigraphy. *Sed. Rev.* **1,** 51–72.

Vail, P.R., Mitchum, R.M. and **Thompson, S.** (1977) Seismic stratigraphy and global changes of sea level, part 3: relative changes of sea level from coastal onlap. In: *Seismic Stratigraphy – Applications to Hydrocarbon Exploration* (Ed. C.E. Payton), *AAPG Mem.*, **26,** 63–81.

Van Keer, I., Muchez, P.H. and **Viaene, W.** (1998) Clay mineralogical variations and evolutions in sandstone sequences near a coal seam and shales in the Westphalian of the Campine Basin (NE Belgium). *Clay Minerals*, **33,** 159–169.

Veizer, J., Bruckschen, P., Pawellek, F., Diener, A., Podlaha, O.G., Carden, G.A.F., Jasper, T., Korte, C., Strauss, H., Azmy, K. and **Ala, D.** (1997) Oxygen isotope evolution of Phanerozoic seawater. *Palaeogeogr., Palaeoclimatol., Palaeoecol.*, **132,** 159–172.

Zalan, P.V., Wolff, S., Astolfi, M.A.M., Santos, V.I., Conceição, J.C.J., Appi, V.T., Neto, E.V.S., Cerqueira, J.R. and **Marques, A.** (1990) The Paraná Basin, Brazil. In: *Interior Cratonic Basins* (Eds M.W. Leighton, D.R. Kolata, D.F. Oltz and J.J. Eidel), *AAPG Mem.*, **51,** 681–708.

Manuscript received 1 August 2002;
revision accepted 12 March 2003.